

RASCBEC: Raman Spectroscopy Calculation via Born Effective Charge

Rui Zhang,^{1,2} Jun Jiang,^{1,2} Alec Mishkin,^{1,2} James N. Fry,¹ and Hai-Ping Cheng^{1,2,*}

¹*Department of Physics, University of Florida, Gainesville, Florida 32611*

²*Quantum Theory Project, University of Florida, Gainesville, Florida 32611*

(Dated: March 21, 2023)

We present a new method to calculate Raman intensity from density functional calculations: the RASCBEC. This method uses the Born effective charge (BEC) instead of the macroscopic dielectric tensor used in the conventional method. This approach reduces the computational time tremendously for molecular crystals or large amorphous systems, decreasing the computational process cost by a factor of $N/8$, where N is the total number of atoms in the simulation unit cell. When N is larger than 8, our method shows advantage over conventional methods. A first test of the new method on the crystal GeO_2 yields results in good agreement with both the conventional theoretical method and experimental data. The effect of varying electric field strength used to compute numerically the derivative of the Born effective charge by electric field, is also tested and summarized. We then apply RASCBEC to a large magnetic molecular crystal that has 448 atoms in a unit cell and to an amorphous Ta_2O_5 sample that has 350 atoms. Consistency among the results calculated with our method, the conventional method, and experimental data remains. Timing information of the two methods is provided, and we clearly see that RASCBEC saves tremendous computation time.

I. INTRODUCTION

Raman spectroscopy reveals information on the vibrational states of atoms from their scattered radiation [1]. With improved performance and sensitivity, it could be used to probe the electronic structure of a single molecule, explore structures of large molecular systems and even help the diagnosis of cancer [2–4].

Theoretical Raman predictions, as a complement to the measurement, can be obtained from first-principles calculations using the macroscopic dielectric tensor [5]. Accurate and reliable, this method has been successfully applied to many kinds of materials [6–8], with the only drawback that huge computational resources are required when applied to large systems. We can do a rough estimation: For a system containing N atoms, $6N - 6$ dielectric tensors need to be determined with either a finite difference method or perturbation theory; and each dielectric tensor requires calculating the linear response in three directions, so we need at least $18N - 18$ self-consistent field (SCF) calculations. We know a typical energy calculation with Density Functional Theory (DFT) [9] scales as $O(n^3)$ and Hartree-Fock (HF) [10] scales as $O(n^4)$ [11], where n is the number of basis functions employed. Therefore, Raman calculations for large systems require considerable CPU time, memory, and/or disk space.

To overcome the computational power requirements, several alternate routes have been proposed, with researchers focusing on three aspects: mathematical formulations, accelerating the first-principle calculations, and finding more effective parallelization methods. For example, among efforts trying to improve the mathemati-

cal foundation, Lazzeri and Mauri [12] proposed replacing the linear response by a second order derivative of the electronic density matrix with respect to a uniform electric field, and they successfully obtained a theoretical Raman spectrum for zeolite (H-ZSM-18), which has 102 atoms. Efforts to accelerate first-principles calculations include the density-fitting (DF) approximation [13, 14], which could reduce the scaling of HF computational effort from $O(n^4)$ to $O(n)$ by localizing the orbitals in each iteration and performing separate fits for each orbital; and also the Resolution of Identity (RI) approximation [15], which could save up to 6.5-fold in CPU time for systems with about 1000 atoms without any significant loss of accuracy by partitioning the electronic Coulomb term in density functional methods into near- and far-field parts. The most popular direction is to find a more effective parallelization method. Many local and fragment-based methods have been proposed [16–18] for this purpose. The central theme of all fragmentation-based methods is to divide the parent system into subsystems such that the latter can be readily treated computationally. A benchmark of fragment-based Raman calculations on test cases containing 36–176 atoms has been done by Khire *et al.* [19], with different levels of theory applied: HF, DFT, and Møller-Plesset second-order perturbation theory (MP2) [20].

In this paper we present the foundations and several tests of our new method to obtain computed Raman spectra using the Born effective charge instead of the macroscopic dielectric tensor, a method that preserves the level of accuracy but reduces the computation cost by a factor of $N/8$. In Section II we describe in detail our algorithm. In Section III we test the method first on a crystal with a six-atom unit cell and then on a magnetic molecule with 448 atoms, and finally we apply it to a 350-atom sample of amorphous Ta_2O_5 . Section IV contains a final conclusion.

* hping@ufl.edu

II. THE RASCBEC METHOD

The conventional method calculates non-resonant first order Raman activity $I_{\text{Raman},s}$ by the change in the polarizability tensor α_s along the mode eigenvectors Q_s for each phonon mode s within the Placzek approximation [5],

$$I_{\text{Raman},s} = \text{const} (\omega_L - \omega_s)^4 \frac{\hbar}{2\omega_s} \left| \hat{e}_i \frac{\partial \alpha_s}{\partial Q_s} \hat{e}_j \right|^2 (1 + \bar{n}_s), \quad (1)$$

where $\bar{n}_s = [\exp(\hbar\omega_s/k_B T) - 1]^{-1}$ is the mean occupation number of the phonon mode s , ω_L is the frequency of the incident light, ω_s is the frequency of phonon mode s , and \hat{e}_i and \hat{e}_j are the unit vectors of the electric field direction (polarization) for the scattered and the incident light.

One recasts the numerical calculation of the polarizability tensor α_s in terms of the macroscopic high-frequency dielectric constant ε_s^∞ [21],

$$I_{\text{Raman},s} \propto \left| \frac{\partial \alpha_s}{\partial Q_s} \right|^2 \equiv \left| \frac{\partial \varepsilon_s^\infty}{\partial Q_s} \right|^2 \approx \left| \frac{\Delta \varepsilon_s^\infty}{\Delta Q_s} \right|^2, \quad (2)$$

and computes the Raman activity using the central-difference scheme

$$I_{\text{Raman},s,ij} \propto \left| \frac{\varepsilon_{s,ij}^\infty(+\delta) - \varepsilon_{s,ij}^\infty(-\delta)}{2\delta} \right|^2, \quad (3)$$

where $\varepsilon_{s,ij}^\infty(\pm\delta)$ are the components of the dielectric tensor ε_s^∞ evaluated at positive and negative displacements $\delta \equiv \Delta Q_s$ along the mode s . For a system containing N atoms, to obtain its Raman intensities we need to compute $6N$ dielectric tensors in total. We can see this from Eqs. (1) to (3), where N atoms will produce $3N$ phonon modes, and the dielectric tensor calculation for each mode requires atomic displacements in both positive and negative directions. When N is large, the computation time for this method is considerable.

Here we introduce our new approach to greatly speed up the procedure for obtaining Raman intensity when N is a large number. The key is to avoid the factor N in the number of calculations. To do this, in Eq. (1) we rewrite the polarizability tensor using the derivative of the polarization by the electric field and then exchange the order of this derivative sequence, taking the derivative first by eigenvector and then by the electric field. The change in macroscopic polarization with respect to the displacement $\xi_{t,j}$ of a given ion/atom t in the j -direction is called the Born effective charge (BEC) tensor, with elements

$$Z_{ij,t} = \frac{\partial P_i}{\partial \xi_{t,j}}, \quad (4)$$

the change of polarization P_i in the i -direction with respect to the displacement $\xi_{t,j}$ of atom t in the j -direction.

Both polarization and BEC are built-in capabilities of the Vienna Ab-initio Simulation Package (VASP) [22, 23] package.

Equivalently, the BEC is also the derivative of the Hellman-Feynman force \mathbf{F} in the i -direction on atom t with respect to the external electric field \mathbf{E} in the j -direction,

$$Z_{t,ij} = \frac{\partial F_{t,i}}{\partial E_j}, \quad (5)$$

so we can simply connect the polarizability tensor to the BEC as

$$\frac{\partial \alpha_{ij}}{\partial \xi_{kt}} = \frac{\partial^2 P_i}{\partial \xi_{kt} \partial E_j} = \frac{\partial Z_{ikt}}{\partial E_j}; \quad (6)$$

and,

$$\frac{\partial \alpha_{ij}}{\partial Q_s} = \sum_k \sum_t \frac{\partial \alpha_{ij}}{\partial \xi_{kt}} \frac{\partial \xi_{kt}}{\partial Q_s} = \sum_k \sum_t \frac{\partial Z_{ikt}}{\partial E_j} \frac{\partial \xi_{kt}}{\partial Q_s}. \quad (7)$$

From Eq. (2), we then get a new expression to calculate Raman activity,

$$I_{\text{Raman},s} \propto \left| \frac{\partial \alpha_s}{\partial Q_s} \right|^2 = \left| \sum_k \sum_t \frac{\partial Z_{ikt}}{\partial E_j} \frac{\partial \xi_{kt}}{\partial Q_s} \right|^2, \quad (8)$$

where $\partial \xi_{kt}/\partial Q_s$ is nothing but a coordinate transform. The challenging part lies in computing the derivative of the BEC with respect to electric field. The BEC of each atom is a 3×3 matrix and electric field is a 3×1 vector, so the derivative is a $3 \times 3 \times 3$ tensor,

$$\frac{\partial Z_{ik}}{\partial E_j} = \frac{\partial^2 F_i}{\partial E_j \partial E_k} \quad (9)$$

With the symmetry in E_j and E_k this tensor has 18 independent components. Recall that the BEC Z_{ij} is the derivative of the Hellman-Feynman force and can be computed using a finite difference method. By converging the charge density for the three electric fields, $\mathbf{E} = (\Delta, 0, 0)$, $\mathbf{E} = (0, \Delta, 0)$, and $\mathbf{E} = (0, 0, \Delta)$, we can express the BEC by expanding the Hellman-Feynman force in a power series in electric field \mathbf{E} ,

$$Z_{ij} = \frac{F_i(\mathbf{E}) - F_i(0)}{\Delta} = \frac{\partial F_i}{\partial E_j} + \frac{1}{2} \frac{\partial^2 F_i}{\partial E_j^2} \Delta + \frac{1}{6} \frac{\partial^3 F_i}{\partial E_j^3} \Delta^2 \quad (10)$$

where to third order

$$\mathbf{F}(\mathbf{E}) = \mathbf{F}(0) + \frac{\partial \mathbf{F}}{\partial \mathbf{E}} \cdot \mathbf{E} + \frac{1}{2} \frac{\partial^2 \mathbf{F}}{\partial \mathbf{E} \partial \mathbf{E}} \cdot \mathbf{E} \cdot \mathbf{E} + \frac{1}{6} \frac{\partial^3 \mathbf{F}}{\partial \mathbf{E} \partial \mathbf{E} \partial \mathbf{E}} \cdot \mathbf{E} \cdot \mathbf{E} \cdot \mathbf{E}. \quad (11)$$

Symmetrically, for electric fields $\mathbf{E} = (-\Delta, 0, 0)$, $\mathbf{E} = (0, -\Delta, 0)$, and $\mathbf{E} = (0, 0, -\Delta)$, the BEC $Z_{i,-j}$ can be written as

$$Z_{i,-j} = \frac{\partial F_i}{\partial E_j} - \frac{1}{2} \frac{\partial^2 F_i}{\partial E_j^2} \Delta + \frac{1}{6} \frac{\partial^3 F_i}{\partial E_j^3} \Delta^2, \quad (12)$$

where the index $-j$ denotes applying the electric field in the negative- j direction. Then some of the components of the derivative tensor can be immediately computed,

$$\frac{\partial Z_{ij}}{\partial E_j} = \frac{\partial^2 F_i}{\partial E_j^2} = \frac{Z_{ij} - Z_{i,-j}}{\Delta} \quad (13)$$

Note that in eq. (13) the second index of Z_{ij} must be the same as the index of E_j because in each derivative the change in the electric field is always along the same direction. Equation (13) accounts for 9 of 27 needed components.

Because VASP applies an electric field to a system in the x , y , z directions sequentially, not simultaneously, we cannot in VASP invoke an electric field in a diagonal direction. Instead, to compute off-diagonal terms, we rotate the lattice within, say, the xy plane by $-\pi/4$ and calculate BEC again with new $E' = (\sqrt{2}\Delta, 0, 0)$, where x' is in the horizontal direction in the rotated frame but is diagonal in the xy plane relative to the original lattice. We then have,

$$Z_{zx'} = \frac{F_z(\approx E') - F_z(0)}{\sqrt{2}\Delta} \quad (14)$$

In the coordinate system of lattice vectors the electric field is actually $\mathbf{E}' = (\Delta, \Delta, 0)$, therefore in the original coordinate system, the BEC calculated can be expressed as

$$Z_{zx'} = \frac{F_z(\Delta, \Delta, 0) - F_z(0, 0, 0)}{\sqrt{2}\Delta} \quad (15)$$

By expanding $F_z(\Delta, \Delta, 0)$ to second order in Δ , we have (suppressing extra 0 arguments)

$$\begin{aligned} F_z(\Delta, \Delta, 0) &= F_z(0) + \left(\frac{\partial F_z}{\partial E_x} + \frac{\partial F_z}{\partial E_y} \right) \Delta \\ &+ \left(\frac{1}{2} \frac{\partial^2 F_z}{\partial E_x^2} + \frac{1}{2} \frac{\partial^2 F_z}{\partial E_y^2} + \frac{\partial^2 F_z}{\partial E_x \partial E_y} \right) \Delta^2 + O(\Delta^3) \\ &= F_z(0) + (Z_{zx} + Z_{zy})\Delta + \frac{\partial Z_{zx}}{\partial E_y} \Delta^2 + O(\Delta^3) \end{aligned} \quad (16)$$

Similarly,

$$\begin{aligned} F_z(-\Delta, -\Delta, 0) &= F_z(0) \\ &- (Z_{z,-x} + Z_{z,-y})\Delta + \frac{\partial Z_{zx}}{\partial E_y} \Delta^2 + O(\Delta^3) \end{aligned} \quad (17)$$

From these we obtain an expression for $Z_{i,\pm j}$ evaluated from the finite difference between field values at $\pm\Delta$ and 0.

$$\begin{aligned} Z_{zx'} - Z_{z,-x'} &= \frac{[F_z(\Delta, \Delta, 0) + F_z(-\Delta, -\Delta, 0) - 2F_z(0)]}{\sqrt{2}\Delta} \\ &= \sqrt{2} \frac{\partial Z_{zx}}{\partial E_y} \Delta + \frac{1}{\sqrt{2}} (Z_{zx} - Z_{z,-x} + Z_{zy} - Z_{z,-y}). \end{aligned} \quad (18)$$

Two more elements in the derivative tensor can be found from Eqs. (15) to (19),

$$\begin{aligned} \frac{\partial Z_{zx}}{\partial E_y} = \frac{\partial Z_{zy}}{\partial E_x} &= [\sqrt{2}(Z_{zx'} - Z_{z,-x'}) - Z_{zx} \\ &+ Z_{z,-x} - Z_{zy} + Z_{z,-y}]/2\Delta \end{aligned} \quad (19)$$

The force in the new x direction now becomes

$$F_{x'} = \frac{F_x + F_y}{\sqrt{2}}. \quad (20)$$

Following the same procedure, we got

$$\begin{aligned} Z_{x'x'} - Z_{x',-x'} &= \frac{[F_{x'}(\Delta, \Delta, 0) + F_{x'}(-\Delta, -\Delta, 0) - 2F_{x'}(0)]}{\sqrt{2}\Delta} \\ &= \left(\frac{\partial Z_{xx}}{\partial E_y} + \frac{\partial Z_{yx}}{\partial E_y} \right) \Delta + \frac{1}{2} (Z_{xx} - Z_{x,-x} + Z_{xy} \\ &- Z_{x,-y} + Z_{yx} - Z_{y,-x} + Z_{yy} - Z_{y,-y}). \end{aligned} \quad (21)$$

Likewise,

$$F_{y'} = -\frac{F_x - F_y}{\sqrt{2}}, \quad (22)$$

and

$$\begin{aligned} Z_{y'x'} - Z_{y',-x'} &= \frac{[F_{y'}(\Delta, \Delta, 0) + F_{y'}(-\Delta, -\Delta, 0) - 2F_{y'}(0)]}{\sqrt{2}\Delta} \\ &= -\left(\frac{\partial Z_{xx}}{\partial E_y} - \frac{\partial Z_{yx}}{\partial E_y} \right) \Delta - \frac{1}{2} (Z_{xx} - Z_{x,-x} + Z_{xy} \\ &- Z_{x,-y} - Z_{yx} + Z_{y,-x} - Z_{yy} + Z_{y,-y}). \end{aligned} \quad (23)$$

Then we will be able to calculate four more elements in the derivative tensor,

$$\begin{aligned} \frac{\partial Z_{xx}}{\partial E_y} = \frac{\partial Z_{xy}}{\partial E_x} &= (Z_{x'x'} - Z_{x',-x'} - Z_{y'x'} + Z_{y',-x'} \\ &- Z_{xx} + Z_{x,-x} - Z_{xy} + Z_{x,-y})/2\Delta \end{aligned} \quad (24)$$

$$\begin{aligned} \frac{\partial Z_{yy}}{\partial E_x} = \frac{\partial Z_{yx}}{\partial E_y} &= (Z_{x'x'} - Z_{x',-x'} + Z_{y'x'} - Z_{y',-x'} \\ &- Z_{yx} + Z_{y,-x} - Z_{yy} + Z_{y,-y})/2\Delta \end{aligned} \quad (25)$$

We see that one rotation can produce the six components zxy , zyx , xyx , xyx , yyx , and yyx . Similar rotations between the xz and yz axes will produce the remaining twelve components. If we rotate the original lattice within the yz plane by $-\pi/4$ then calculate BEC again with new $E''_y = \sqrt{2}\Delta$, where y'' is the y direction in the rotated coordinates,

$$\frac{\partial Z_{xy}}{\partial E_z} = \frac{\partial Z_{xz}}{\partial E_y} = [\sqrt{2}(Z_{xy'} - Z_{x,-y'}) - Z_{xy} + Z_{x,-y}) - Z_{xz} + Z_{x,-z}]/2\Delta \quad (26)$$

$$\frac{\partial Z_{yy}}{\partial E_z} = \frac{\partial Z_{yz}}{\partial E_y} = (Z_{y'y'} - Z_{y',-y'} - Z_{z'y'} + Z_{z',-y'} - Z_{yy} + Z_{y,-y} - Z_{yz} + Z_{y,-z})/2\Delta \quad (27)$$

$$\frac{\partial Z_{zy}}{\partial E_z} = \frac{\partial Z_{zz}}{\partial E_y} = (Z_{y'y'} - Z_{y',-y'} + Z_{z'y'} - Z_{z',-y'} - Z_{zy} + Z_{z,-y} - Z_{zz} + Z_{z,-z})/2\Delta \quad (28)$$

Similarly again we rotate the lattice within the zx plane by $-\pi/4$ then calculate BEC with $E_{z''} = \sqrt{2}\Delta$, where z'' is the z direction in the rotated coordinates. Then,

$$\frac{\partial Z_{yz}}{\partial E_x} = \frac{\partial Z_{yx}}{\partial E_z} = [\sqrt{2}(Z_{yz'} - Z_{y,-z'}) - Z_{yx} + Z_{y,-x}) - Z_{yz} + Z_{y,-z}]/2\Delta \quad (29)$$

$$\frac{\partial Z_{zz}}{\partial E_x} = \frac{\partial Z_{zx}}{\partial E_z} = [Z_{z'z'} - Z_{z',-z'} - Z_{x'z'} + Z_{x',-z'} - Z_{zz} + Z_{z,-z} - Z_{zx} + Z_{z,-x}]/2\Delta \quad (30)$$

$$\frac{\partial Z_{xz}}{\partial E_x} = \frac{\partial Z_{xx}}{\partial E_z} = [Z_{z'z'} - Z_{z',-z'} + Z_{x'z'} - Z_{x',-z'} - Z_{xz} + Z_{x,-z} - Z_{xx} + Z_{x,-x}]/2\Delta \quad (31)$$

By now all elements of the derivative tensor in Eq. (9) have been obtained and we can compute the Raman intensity tensor immediately once the BECs are ready. BECs along the x , y , z directions can be computed in a single calculation with unrotated system to save computation time. And so are BECs along the $-x$, $-y$, $-z$ directions. The calculation using the rotated system yields BECs along the xy , yz , xz directions, in both positive and negative directions, respectively. So altogether the calculations yield 8 BECs. Compared to the $6N$ dielectric tensors that are needed with the conventional method, a substantial saving of computation time is effected.

III. VALIDATION OF THE RASCBEC METHOD

The rutile type of GeO_2 with a six-atom unit cell [24] is used as the first test sample to validate RASCBEC. We perform phonon calculations first, obtaining phonon frequencies and eigenvectors from the diagonalization of the dynamical matrix. Then both dielectric tensors and BECs are obtained using VASP.

Comparison of RASCBEC with the conventional method is shown in Figure 1. The experimental Raman spectrum of rutile GeO_2 measured at 298 K [25] is also included. We can see that the calculated Raman spectra from both calculational methods exhibit the same two-peak features measured in experiment, but the peak positions are shifted to higher frequencies, as marked by

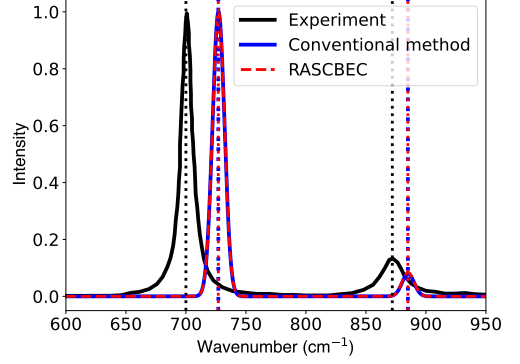


FIG. 1. Raman spectra of rutile GeO_2 calculated from the conventional method and RASCBEC (right) compared with experimental Raman (ref. [25]) (left).

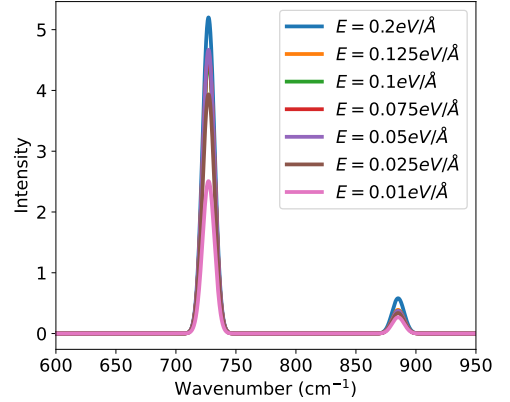


FIG. 2. Raman spectra of rutile GeO_2 calculated using different electric fields.

dotted line in Figure 1. The experiment measures two peaks at 700 cm^{-1} and 872 cm^{-1} and from calculation the two peaks are at 727 cm^{-1} and 885 cm^{-1} . RASCBEC gives the same result as the conventional method, except that the peak heights differ slightly.

One limit on accuracy is the numerical derivative by electric field. If the applied electric field Δ is too small, the error will be dominated by DFT convergence and round-off errors, but if the field is too large, higher order finite difference errors will become large. A test of the Raman spectra calculated for electric field strengths ranging from 0.025 eV/\AA to 0.2 eV/\AA is shown in Figure 2. It can be seen that relative intensities of the Raman peaks vary with the strength of electric field applied. How the intensity varies with electric field strength is shown in Figure 3 and Figure 4. There is a flat region from 0.05 eV/\AA to 0.125 eV/\AA , which means that in this region the computational result is robust. The result shown in Figure 1 used electric field $E = 0.1 \text{ eV/\AA}$.

Timing information for the two methods is provided

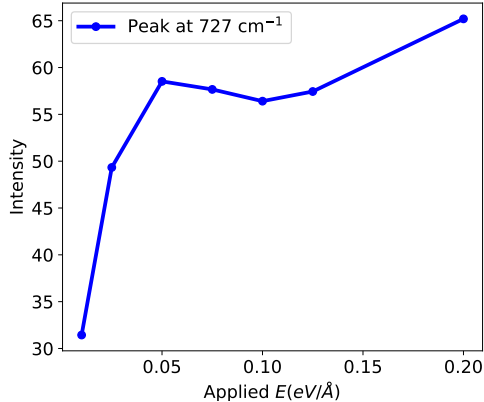


FIG. 3. First peak height variation with electric field.

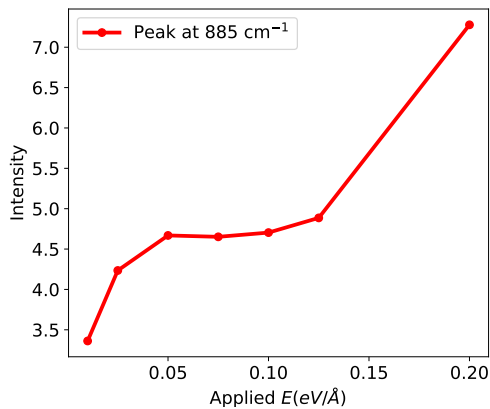


FIG. 4. Second peak height variation with electric field.

in Table I. Note that the estimated time for calculating ϵ or Z given in the table should be viewed as an upper limit, since all BEC calculations subsequent to the first one take less time. This is because after rotation, only one direction of the electric field needs to be applied instead of 3. The Vienna Ab-initio Simulation Package (VASP)[22, 23] is employed for all first principle calculations. All computations are performed on AMD EPYC 7702.

The conventional method calculates the static ion-clamped dielectric matrix using density functional perturbation theory. For a system containing N atoms, there are $3(N-1)$ phonon modes. Two dielectric tensors need to be generated for each phonon mode, displacing the structure in opposite directions, so $2 \times 3 \times (N-1) = 6N - 6$ dielectric tensor calculations are needed in total. When $N = 6$, this number is 30.

The RASCBEC method differentiating the Born effective charge displaces an electric field in the positive and negative x , y , z directions as well as the xy , yz , and xz directions. Since BECs along the x , y , z directions can be computed in a single calculation, and $-x$, $-y$, $-z$ in

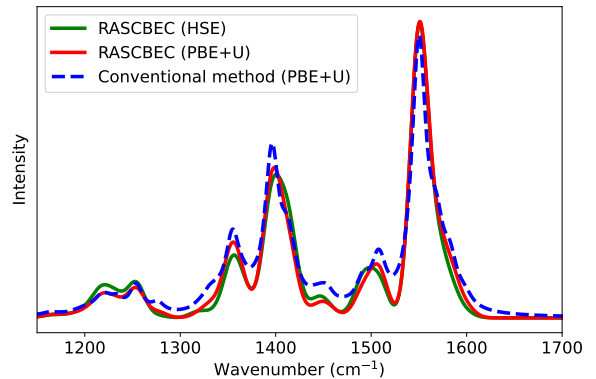


FIG. 5. Calculated Raman spectra of Fe₂SCO using both the conventional method and RASCBEC

another single calculation, 8 BEC are needed in total. This number is independent of N .

In summary, if the system size scales to N atoms, then the conventional method will need to generate $6(N-1)$ dielectric tensors. The RASCBEC method needs 8 BEC calculations with electric field applied along different directions. Each BEC calculation with an electric field applied takes about 18 times longer than one without an electric field. Therefore the time ratio of convention method and RASCBEC is $N/8$. When N is greater than 8, RASCBEC has an advantage in computation time.

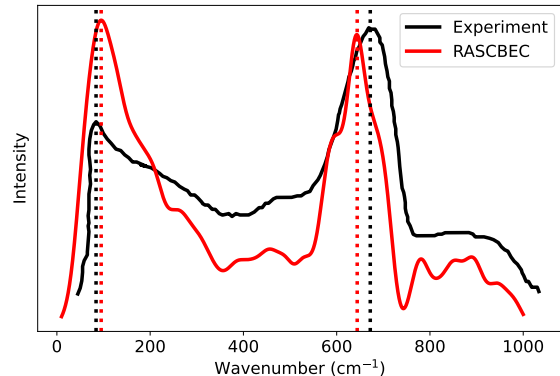
To demonstrate its advantage for large systems, we then apply both the RASCBEC method and conventional method to a large magnetic molecule containing 448 atoms, a recently developed and easily sublimable SCO material, $[Fe(tBu_2qsal)_2]$ [26]. The computed Raman spectra of this molecule's low spin state are shown in Figure 5. Red and green lines are the Raman spectra calculated using RASCBEC. To produce the red curve we use PBE+ U to calculate BEC, as for the green curve we use hybrid functional. For both ways we applied the electric field $E = 0.05$ eV/Å. The intensities of these two spectra are normalized with the same normalization factor to compare with a Raman spectra calculated using the conventional method [26]. One can see that in Figure 5 all three curves share the same peak features, in terms of the phonon frequency corresponding to each peak and the relative intensity in general among the peaks. However, one can still identify differences existing at some frequencies. We know that analytically RASCBEC and the conventional method are equivalent. We suspect that this difference comes from the finite differences used to compute derivatives numerically, the derivative of the dielectric tensor for the conventional method and the derivative of the BEC for RASCBEC. When calculating derivatives, all numerical methods make approximations. In solids, these approximations are likely more reliable than in molecules. In molecules, some modes may have substantially large vibrations, and anharmonic effects may become large. However, even when there is strong anhar-

TABLE I. Timing of two methods on crystal (6 atoms)

$N = 6$	Number of modes or Z	Average time of getting 1 ϵ or Z	Total time
Dielectric tensor (ϵ)	$6(N - 1) = 30$	1,700 sec (1 cpu)	51,000 sec
BEC (Z)	8	24,886 sec (1 cpu)	200,000 sec

TABLE II. Timing of two methods on magnetic molecule (448 atoms)

$N = 448$	Number of modes or Z	Average time of getting 1 ϵ or Z	Total time
Dielectric tensor (ϵ)	$6(N - 1) = 2682$	20,450 sec (32 cpu)	54,846,900 sec
BEC (Z)	8	122,860 sec (32 cpu)	982,880 sec

FIG. 6. Calculated Raman spectra of amorphous Ta_2O_5 using RASCBECC compared with experiment data [27].

monicity, we can choose the electric field strength such that response to the electric field is still approximately linear. We see this explicitly in Figures 3 and 4 when the electric field becomes large.

Timing information for two methods is provided in Table II. All computations are performed on AMD EPYC 7702. The Vienna Ab-initio Simulation Package (VASP) [22, 23] is employed for all first-principle calculations. Regarding the total computation cost, ratio between conventional method and RASCBECC is $54846900/982880 = 55.8$, and the predicted ratio is $N/8 = 448/8 = 56$. We see that RASCBECC is able to save a factor of 56 in computation time for a 448-atom molecule and yet produce Raman spectra with the same accuracy.

Finally we test RASCBECC on large and complex systems: the amorphous materials. Performing thousands of first principle calculations on a large and disordered system can be a daunting task due to the huge computational cost, fortunately we have RASCBECC to handle it. The material we use is Ta_2O_5 . An amorphous sample containing 350 atoms is prepared by Molecular Dynamics (MD) simulation using melt-quench method. Classical MD simulation code LAMMPS[28] is used to run the simulation. A classical potential formulated by Trinastic *et al.* [29] is used to model inter-atomic potential in Ta_2O_5 .

The calculated and experimental Raman spectra [27] are shown in Figure 6. The black curve is the experiment measurement and the red curve is the Raman spectrum calculated using RASCBECC. Peak positions are denoted with dotted lines. We can clearly see that they both have two main peaks, and the peak positions are very close. In the experiment, the first and second peaks are measured at 84 cm^{-1} and 672 cm^{-1} while from calculation they are at 95 cm^{-1} and 644 cm^{-1} . The computation time of one BEC on AMD EPYC 7702 is about 65,540 secs on 256 cpu, so the total cost is 524,320 secs. To have a taste of the conventional method on amorphous materials, we also tried one dielectric tensor calculation and it takes 52,170 secs on 256 cpu. 2094 such calculations are needed so the total required computation time is about 109,243,980 secs. This is much too expensive to carry through to the finish.

IV. CONCLUSION

In conclusion, in this paper we have introduced a newly developed method of calculation of Raman spectra using an electric field derivative of the Born effective charge to replace the sum over phonon modes of polarizability derivatives along mode eigenvectors used in the conventional method. We call the new method the RASCBECC. Since for large systems there is a large number of terms in the polarizability sum, this allows us to expedite first-principles Raman calculation and probe large systems in an economical way. This method saves computation time for large systems by a factor of $N/8$, where N is the number of atoms in the simulation box. Tests of the RASCBECC method on an atomic crystal, a large magnetic molecule, and a large amorphous system verify its ability to reproduce the results of the conventional method and its significant reduction in computational cost. Applying this method to even larger and more complex systems to calculate Raman activity is possible, and we will explore more directions in the future.

ACKNOWLEDGMENTS

This work is supported by the National Science Foundation (NSF) LIGO program through Grants No.

2011770 and No. 2011776. Computations were performed using the utilities of the National Energy Research Scientific Computing Center and the University of Florida Research Computing HiPerGator.

-
- [1] D. A. Long, Raman spectroscopy, New York **1** (1977).
- [2] B. Schrader, *Infrared and Raman spectroscopy: methods and applications* (John Wiley & Sons, 2008).
- [3] N. Colthup, *Introduction to infrared and Raman spectroscopy* (Elsevier, 2012).
- [4] E. Smith and G. Dent, *Modern Raman spectroscopy: a practical approach* (John Wiley & Sons, 2019).
- [5] D. Porezag and M. R. Pederson, Infrared intensities and raman-scattering activities within density-functional theory, *Phys. Rev. B* **54**, 7830 (1996).
- [6] T. Sahu, A. Bhattacharyya, and A. N. Gandi, Raman spectra characterization of boron carbide using first-principles calculations, *Physica B: Condensed Matter* **633**, 413738 (2022).
- [7] G. Roma, K. Gillet, A. Jay, N. Vast, and G. Gutierrez, Understanding first-order raman spectra of boron carbides across the homogeneity range, *Phys. Rev. Materials* **5**, 063601 (2021).
- [8] Z. Deng, Z. Li, W. Wang, and J. She, Vibrational properties and raman spectra of pristine and fluorinated blue phosphorene, *Phys. Chem. Chem. Phys.* **21**, 1059 (2019).
- [9] D. Sholl and J. A. Steckel, *Density functional theory: a practical introduction* (John Wiley & Sons, 2011).
- [10] C. F. Fischer, *Hartree-Fock method for atoms. A numerical approach* (John Wiley and Sons, Inc., New York, 1977).
- [11] D. L. Strout and G. E. Scuseria, A quantitative study of the scaling properties of the hartree-fock method, *The Journal of chemical physics* **102**, 8448 (1995).
- [12] M. Lazzeri and F. Mauri, First-principles calculation of vibrational raman spectra in large systems: Signature of small rings in crystalline SiO₂, *Physical review letters* **90**, 036401 (2003).
- [13] H.-J. Werner, F. R. Manby, and P. J. Knowles, Fast linear scaling second-order møller-plesset perturbation theory (mp2) using local and density fitting approximations, *The Journal of Chemical Physics* **118**, 8149 (2003), <https://doi.org/10.1063/1.1564816>.
- [14] R. Polly, H.-J. Werner, F. R. Manby, and P. J. Knowles, Fast hartree-fock theory using local density fitting approximations, *Molecular Physics* **102**, 2311 (2004), <https://doi.org/10.1080/0026897042000274801>.
- [15] M. Sierka, A. Hogekamp, and R. Ahlrichs, Fast evaluation of the coulomb potential for electron densities using multipole accelerated resolution of identity approximation, *The Journal of Chemical Physics* **118**, 9136 (2003), <https://doi.org/10.1063/1.1567253>.
- [16] M. A. Collins and R. P. Bettens, Energy-based molecular fragmentation methods, *Chemical reviews* **115**, 5607 (2015).
- [17] K. Raghavachari and A. Saha, Accurate composite and fragment-based quantum chemical models for large molecules, *Chemical reviews* **115**, 5643 (2015).
- [18] S. Li, W. Li, and J. Ma, Generalized energy-based fragmentation approach and its applications to macromolecules and molecular aggregates, *Accounts of Chemical Research* **47**, 2712 (2014), pMID: 24873495, <https://doi.org/10.1021/ar500038z>.
- [19] S. Khire, N. Sahu, and S. Gadre, Harnessing desktop computers for ab initio calculation of vibrational ir/raman spectra of large molecules, *Journal of Chemical Sciences* **130** (2018).
- [20] C. Møller and M. S. Plesset, Note on an approximation treatment for many-electron systems, *Phys. Rev.* **46**, 618 (1934).
- [21] J. Mitroy, M. S. Safronova, and C. W. Clark, Theory and applications of atomic and ionic polarizabilities, *Journal of Physics B: Atomic, Molecular and Optical Physics* **43**, 202001 (2010).
- [22] G. Kresse and J. Furthmüller, Efficient iterative schemes for ab initio total-energy calculations using a plane-wave basis set, *Phys. Rev. B* **54**, 11169 (1996).
- [23] G. Kresse and J. Furthmüller, Efficiency of ab-initio total energy calculations for metals and semiconductors using a plane-wave basis set, *Comput. Mater. Sci.* **6**, 15 (1996).
- [24] A. A. Bolzan, C. Fong, B. J. Kennedy, and C. J. Howard, Structural studies of rutile-type metal dioxides, *Acta Crystallographica Section B* **53**, 373 (1997), <https://onlinelibrary.wiley.com/doi/pdf/10.1107/S0108768197001468>.
- [25] T. P. Mernagh and L.-g. Liu, Temperature dependence of raman spectra of the quartz-and rutile-types of GeO₂, *Physics and chemistry of minerals* **24**, 7 (1997).
- [26] M. Gakiya-Teruya, X. Jiang, D. Le, O. Ungor, A. J. Durrani, J. J. Koptur-Palenchar, J. Jiang, T. Jiang, M. W. Meisel, H.-P. Cheng, X.-G. Zhang, X.-X. Zhang, T. S. Rahman, A. F. Hebard, and M. Shatruk, Asymmetric design of spin-crossover complexes to increase the volatility for surface deposition, *Journal of the American Chemical Society* **143**, 14563 (2021), pMID: 34472348, <https://doi.org/10.1021/jacs.1c04598>.
- [27] C. Joseph, P. Bourson, and M. D. Fontana, Amorphous to crystalline transformation in Ta₂O₅ studied by raman spectroscopy, *Journal of Raman Spectroscopy* **43**, 1146 (2012), <https://analyticalsciencejournals.onlinelibrary.wiley.com/doi/pdf/10.1002/jrs.3142>.
- [28] S. Plimpton, Fast parallel algorithms for short-range molecular dynamics, *Journal of Computational Physics* **117**, 1 (1995).
- [29] J. P. Trinastic, R. Hamdan, Y. Wu, L. Zhang, and H.-P. Cheng, Unified interatomic potential and energy barrier distributions for amorphous oxides, *The Journal of Chemical Physics* **139**, 154506 (2013), <https://doi.org/10.1063/1.4825197>.